Ligand Non-Innocence

International Edition: DOI: 10.1002/anie.201509099
German Edition: DOI: 10.1002/ange.201509099

Electronic Structure of Copper Corroles

*Christopher M. Lemon, Michael Huynh, Andrew G. Maher, Bryce L. Anderson, Eric D. Bloch, David C. Powers, and Daniel G. Nocera**

Abstract: *The ground state electronic structure of copper corroles has been a topic of debate and revision since the advent of corrole chemistry. Computational studies formulate neutral Cu corroles with an antiferromagnetically coupled Cu^{II} corrole radical cation ground state. X-ray photoelectron spectroscopy, EPR, and magnetometry support this assignment. For comparison, Cu^{II} isocorrole and [TBA][$Cu(CF_3)_4$] were studied as authentic Cu^{II} and Cu^{III} samples, respectively. In addition, the one-electron reduction and one-electron oxidation processes are both ligand-based, demonstrating that the Cu^{II} centre is retained in these derivatives. These observations underscore ligand non-innocence in copper corrole complexes.*

Since the original synthesis of copper corroles,[1] the electronic structure and oxidation state of the copper centre in these compounds has been a topic of debate. The corrole was initially formulated as a Cu^{II} metal centre in a dianionic ligand, where one of the pyrrole nitrogen atoms retains a proton.[1–4] The electronic structure was later revised as a fully deprotonated corrole ligand containing a Cu^{III} centre[5] due to the lack of an *N*-pyrrole proton by IR spectroscopy and crystallography, and the diamagnetic nature of the compound. Subsequent structural[6–10] and computational[11,12] studies of copper corroles with a wide variety of *meso* and β-substituents have suggested the ground state to be best described as an antiferromagnetically coupled Cu^{II} corrole radical cation. These studies have shown that saddling distortions are *inherent* to copper corroles as a consequence of significant overlap between the Cu $d_{x^2-y^2}$ orbital and the corrole π HOMO.[6] However, the electronic structure of copper corroles remains an unresolved issue as a recent report of a one-electron-oxidized Cu corrole derivative was assigned as the first example of a discrete Cu^{IV} species.[13] This conclusion was derived from the assumption that the neutral corrole complex contains a Cu^{III} centre. In this study, we provide comparative spectroscopic and magnetic data of Cu corroles, the corresponding cation and anion, and a Cu isocorrole that establish the presence of Cu^{II} across the series of complexes with the redox load borne by the macrocyclic ligand.

[*] C. M. Lemon, M. Huynh, A. G. Maher, B. L. Anderson, Dr. E. D. Bloch, Prof. Dr. D. G. Nocera
Department of Chemistry and Chemical Biology, Harvard University
12 Oxford Street, Cambridge MA 02138 (USA)
E-mail: dnocera@fas.harvard.edu
Prof. Dr. D. C. Powers
Department of Chemistry, Texas A&M University
College Station, TX 77843-3255 (USA)

Supporting information for this article is available on the WWW under http://dx.doi.org/10.1002/anie.201509099.

The copper complex of corrole **1** (Scheme 1) was prepared following literature methods using $Cu(OAc)_2$ in pyridine[14,15] with an isolated yield comparable to those obtained for other Cu corrole complexes.[6] Brown crystals of **Cu-1** suitable for X-ray diffraction were grown from a toluene solution of the compound. A summary of the crystallographic data is provided in Table S1 in the Supporting Information (SI). Figure 1 shows the crystal structure of one of the two corroles in the asymmetric unit. The metal centre displays a distorted square planar geometry, with d(Cu–N) = 1.883–1.899 Å bond lengths, which is consistent with other Cu corrole structures.[15,16] The corrole adopts the typical nonplanar, saddled geometry,[6,9,10] where alternating pyrrole units point above and below the plane of the macrocycle.

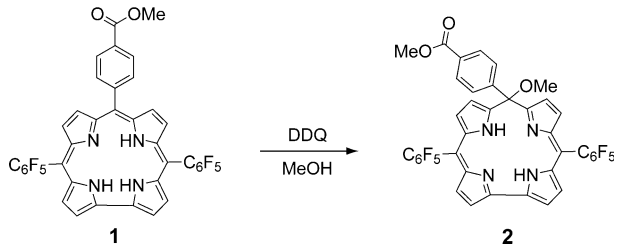

Scheme 1. Conversion of corrole **1** to isocorrole **2**.

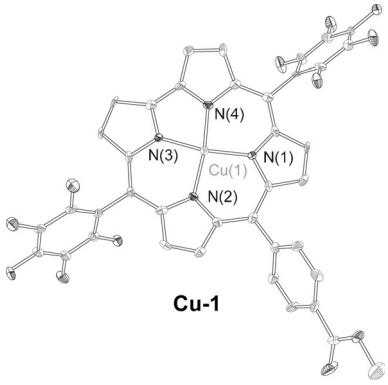

Figure 1. Solid state structure of **Cu-1**. Thermal ellipsoids are drawn at the 50% probability level.

An authentic Cu^{II} reference compound of the corrole in a nearly identical ligand field is obtained by oxidation of **1** followed by attack of methanol[17,18] to furnish the analogous isocorrole **2** (Scheme 1). In the isocorrole, one of the *meso* carbons is sp^3 hybridized, rendering it a non-aromatic dianionic ligand. Metallation of **2** with copper acetate and

mild heating gave **Cu-2** in high yield. The absorption spectra of **2** and **Cu-2** (Figure S1) are consistent with other reports.[17,18] As expected for a Cu^{II} complex, the χT versus T plot (Figure S2) of **Cu-2** is indicative of a typical paramagnet, with magnetic ordering observed at $T < 15$ K.

Cu-1 displays an apparent diamagnetic ^{1}H NMR spectrum at room temperature in $CDCl_3$ and [D_8]toluene (Figure 2 and S3). However, unlike other diamagnetic metallocorroles, only the *meso* aryl protons are well-resolved doublets (at 7.38 and 8.19 ppm). The four β-pyrrole protons (at 7.74, 7.18, 7.13, and 7.10) appear in the 7.1–7.8 ppm region as broad signals. This is in contrast to **Au-1**, a true diamagnetic M^{III} compound, where all of the signals are resolved into clear doublets[19] and display resonances that are similar to those of the free-base **1** (8.6–9.2 ppm).[20] The large spectral shift and the broad signals of **Cu-1** suggest the presence of a paramagnetic species at room temperature. The singlet–triplet equilibrium that gives rise to this paramagnetism may be quantified from VT ^{1}H NMR of **Cu-1** (Figure 2a). Noting that the β-proton signal at 7.74 ppm clearly shifts without interference from other signals over the 25–100 °C range, a fit of the shift of this signal (δ) with temperature (T) to the following equation yields the energy difference ($\Delta E_{T\text{-}S}$) between the triplet and singlet states:[21–23]

$$\delta(\text{ppm}) = \delta_{\text{singlet}} + 10^6 \frac{g\beta_e}{g_N\beta_N}\frac{aS(S+1)}{kT}\left[3 + \exp\left(\frac{\Delta E_{T\text{-}S}}{RT}\right)\right]^{-1} \quad (1)$$

where g and g_N are the electronic and nuclear g-values, respectively, β_e and β_N are the Bohr and nuclear magnetons, respectively, a is the isotropic hyperfine coupling constant, S is the spin of the system ($S = 1$ for a triplet), k is the Boltzmann constant, and R is the gas constant. The fit of the data in Figure 2b to Equation (1) yields $\delta_{\text{singlet}} = 7.42 \pm 0.04$ ppm, $a = 0.152 \pm 0.027$ G, and $\Delta E_{T\text{-}S} = 13.9 \pm 0.7$ kJ mol^{-1} (0.144 ± 0.007 eV); details of the fitting procedure are provided in the Supporting Information. As a means of validating the results of this experiment, **Cu-1** was examined by SQUID magnetometry (Figure 2c) and the data was fit to the following Hamiltonian:

$$\hat{H} = -J\hat{S}_A\cdot\hat{S}_B + \beta\left(\hat{S}_A\cdot g_A + \hat{S}_B\cdot g_B\right)\cdot B \quad (2)$$

where J is the exchange coupling constant, $\hat{S}$ is the spin angular momentum operator, β is the Bohr magneton of the electron, g is the electron g-factor, and B is the applied field; the subscripts A and B refer to the two spin components (metal and ligand) that are coupled. This Hamiltonian accounts for both magnetic exchange (first term) and Zeeman splitting (second term). The plot of χT versus T is indicative of an antiferromagnetically coupled complex with a coupling ($-2J$) of 1236 ± 40 cm^{-1} or 14.8 ± 0.5 kJ mol^{-1} (see SI). We note that this coupling represents the energy difference between the antiferromagnetic (singlet) and ferromagnetic (triplet) states and is identical to $\Delta E_{T\text{-}S}$ of Equation (1). Thus the energy difference between the singlet and triplet states of **Cu-1** as determined from Figure 2b and c are in excellent agreement. Our experimental value of $\Delta E_{T\text{-}S}$ for **Cu-1** shows good agreement with the energy gap predicted by DFT calculations.[11] Using the value of $\Delta E_{T\text{-}S} = 13.9 \pm 0.7$ kJ mol^{-1}, the relative population of the two states can be determined at a given temperature by the Boltzmann factor:

$$\frac{N_T}{N_S} = 3\exp\left(\frac{-\Delta E_{T\text{-}S}}{kT}\right) \quad (3)$$

where N_T and N_S are the populations of the triplet and singlet states, respectively and the factor of 3 accounts for the degeneracy of the triplet state. At 23 °C, only 1.05 % of the **Cu-1** molecules in the sample are in the triplet state; this value increases to 3.29 % at 100 °C. The low population of the triplet state accounts for the seemingly diamagnetic nature of the compound, as well as the broad signals of the β-pyrrole protons due to their proximity to the copper centre.

Figure 3a shows the cyclic voltammogram of **Cu-1**. Two reversible reductions at −0.28 V and −2.15 V versus Fc^+/Fc are observed, as well as a reversible oxidation at +0.55 V and a quasi-reversible oxidation around +1.27 V. The accessibility of the oxidized and reduced species at reasonable potentials allowed for their preparation with mild reagents. Reduced **Cu-1** was obtained using zinc metal in pyridine to give Zn[**Cu-1**]$_2$ as a dark green solution. The oxidized derivative [**Cu-1**][PF_6] was produced by treating **Cu-1** with $AgPF_6$ in CH_2Cl_2 to give a light yellow-brown solution. The reduced corrole exhibits a significant red shift of the Soret band with a concomitant growth of the Q bands. Conversely, the intensity of the Soret band decreases and the Q bands have virtually no intensity for the oxidized corrole (Figure 3b). The reduced corrole is stable in solution on the bench top for several months, while the oxidized corrole has limited stability. Whereas the UV-vis spectrum of a dilute sample of [**Cu-1**][PF_6] in CH_2Cl_2 remains virtually unchanged after 2 hours (Figure S4a), the stock solution turns green over this period of time (Figure S4b) to give a diamagnetic compound

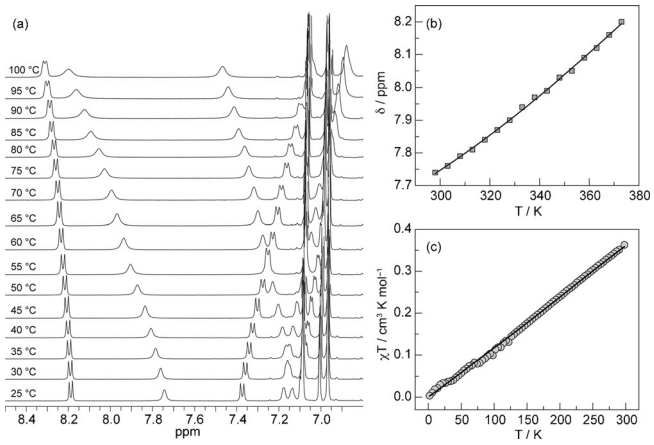

Figure 2. a) Variable temperature ^{1}H NMR spectra of **Cu-1** in [D_8]toluene showing the aromatic region of the spectrum. The large peaks between 6.9 and 7.1 ppm are from toluene. b) Plot of the data from (a), analysing the β pyrrole proton that shifts from 7.74 at 25 °C to 8.20 at 100 °C. c) SQUID magnetometry data for a solid sample of **Cu-1**. The data was fit to Equation (2) and shows that this compound is antiferromagnetic with a coupling ($-2J$) of 1236 cm^{-1}.

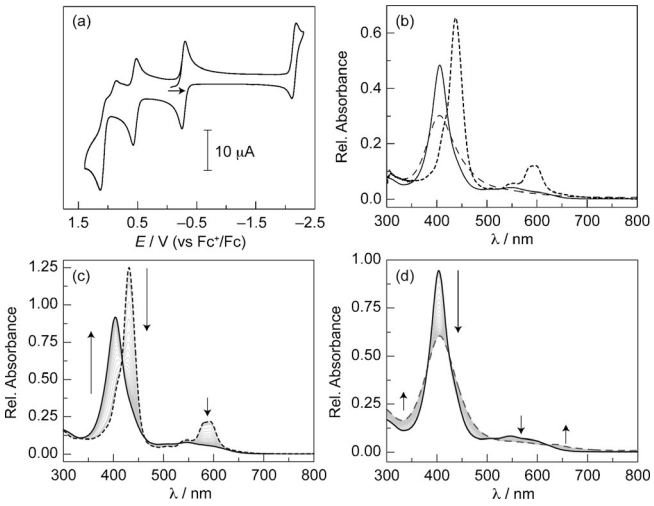

Figure 3. a) Cyclic voltammogram of **Cu-1** in MeCN with 0.1 M [TBA][PF_6] recorded at 100 mV s^{-1}. b) Comparative absorption spectra of **Cu-1** (——), [**Cu-1**][PF_6] (– – –), and Zn[**Cu-1**]$_2$ (-----). c) Spectroelectrochemistry of **Cu-1** showing the conversion of [**Cu-1**]$^-$ (-----) to **Cu-1** (——) using bulk electrolysis at 0 V. d) Spectroelectrochemistry of **Cu-1** showing the conversion of **Cu-1** (——) to [**Cu-1**]$^+$ (– – –) using bulk electrolysis at 0.8 V.

(Figure S5) and, presumably, free copper in solution. Thin-layer spectroelectrochemical experiments (Figure 3c,d) are consistent with the absorption spectra of Zn[**Cu-1**]$_2$ and [**Cu-1**][PF_6].

EPR spectra of **Cu-1** and **Cu-2** provide information regarding the formal oxidation state of the metal centre. As a benchmark, Figure 4a shows the EPR spectrum of **Cu-2.** As expected for a Cu^{II} sample, the spectrum is characteristic of an axial doublet for a single unpaired electron ($S = 1/2$) with

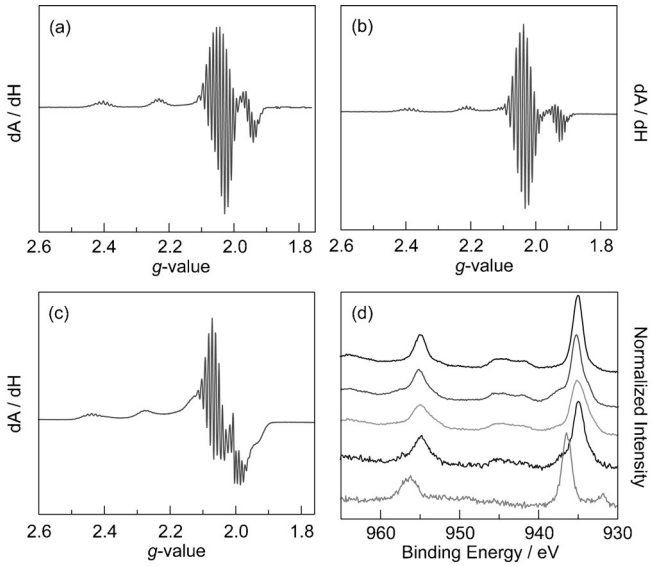

Figure 4. X-band EPR spectra of a) **Cu-2** in 2-Me-THF, b) Zn[**Cu-1**]$_2$ in 2-Me-THF/pyridine, and c) [**Cu-1**][PF_6] in 2-Me-THF/DCM. All spectra were recorded at 77 K. d) The Cu 2p region of the XPS spectra of the compounds and derivatives studied herein, from top to bottom: **Cu-2**, **Cu-1**, Zn[**Cu-1**]$_2$, [**Cu-1**][PF_6], and [TBA][$Cu(CF_3)_4$].

hyperfine coupling to the $^{65}Cu/^{63}Cu$ nucleus ($I = 3/2$) to give a four-line pattern; this signal is further split by ligand superhyperfine coupling to the four ^{14}N nuclei ($I = 1$) of the corrole to give a nine-line pattern. This type of spectrum has been previously observed for the copper complex of a 10-oxacorrole.[6] As expected from the magnetic data, a sample of **Cu-1** in 2-Me-THF is EPR silent. The EPR spectra for Zn[**Cu-1**]$_2$ in pyridine/2-Me-THF (Figure 4b) and [**Cu-1**][PF_6] in DCM/2-Me-THF (Figure 4c) are very similar to **Cu-2**, establishing the presence of a Cu^{II} centre in these compounds. Simulations for these spectra are presented in Figure S6 and the parameters are summarised in Table S2.

X-ray photoelectron spectroscopy (XPS) is particularly diagnostic of the oxidation state in copper complexes, as shake-up satellite peaks are observed in the Cu 2p region of the spectrum for Cu^{II} species, but are absent for Cu^{III} derivatives.[24,25] Figure 4d shows the XPS spectra of the Cu corroles as compared to **Cu-2** and [TBA][$Cu(CF_3)_4$],[26] which were studied as authentic Cu^{II} and Cu^{III} samples, respectively. With the caveat that ligand field inversion for the [$Cu(CF_3)_4$]$^-$ anion leads to a Cu^{I} complex,[27] the XPS data suggests that the metal is in a highly oxidized state, exhibiting Cu 2p binding energies greater than Cu^{II} samples. The derivatives of **Cu-1** and **Cu-2** exhibit broad shake-up satellites between 940.2 and 947.4 eV while [TBA][$Cu(CF_3)_4$] does not. Moreover, the Cu $2p_{3/2}$ peak appears at 935.0 eV for **Cu-2** and all the **Cu-1** corrole derivatives are within 0.1 eV of this peak. This feature is shifted to 936.4 eV for [TBA][$Cu(CF_3)_4$], consistent with a more oxidized Cu centre in this compound. These results further support the presence of Cu^{II} in **Cu-1** and its oxidized and reduced derivatives.

To complement spectroscopic experiments, DFT calculations (B3LYP/6-311G(d,p) with toluene CPCM solvation) were performed for **Cu-1** as a closed shell ^{1}Cu(III) singlet, a ferromagnetically coupled ^{3}Cu(II) corrole radical cation, and an antiferromagnetically coupled, broken symmetry ^{1}Cu(II) corrole radical cation (Tables S3–S5, Figure S7 and S8). The B3LYP functional has been used to study a wide variety of copper complexes[28] and it has been shown for copper corroles to give the most accurate values of $\Delta E_{T\text{-}S}$ when benchmarked against pure functionals or multiconfigurational methods.[11] As a benchmark, energies were also computed for optimized structures using Complete Active Space Multiconfiguration SCF (CASSCF). Both methods predict the broken symmetry singlet ^{1}Cu(II) as the ground state, consistent with experiment, and bound the triplet state +0.0167–0.415 eV higher in energy. This energy range corresponds to the calculated magnetic coupling for **Cu-1**, which is known to be highly dependent on the choice of functional.[11] In addition, comparison of computed geometries to the solid-state structure of **Cu-1** (Figure S9) shows that singlet state calculations match best (i.e., lowest RMS deviation) with the saddled experimental structure, while the calculated triplet state geometry is planar. Doublet and quartet states were calculated for both [**Cu-1**]$^+$ and [**Cu-1**]$^-$ and it was found that the quartet states are higher in energy for both species by 0.132 eV and 1.381 eV, respectively (Tables S6–S9 and Figure S10 and S11). TD-DFT calculations of **Cu-1**, [**Cu-1**]$^-$, and [**Cu-1**]$^+$ (Tables S10–S12 and Fig-

ure S12–S14) provide simulated UV-vis spectra that have qualitative similarities to the experimental spectra (Figure S15) inasmuch as the reduced corrole has red-shifted Q bands relative to **Cu-1** and the oxidized corrole has a less intense Soret band.

The electronic structure of each compound examined in this study is summarised in Figure 5, which presents the calculated spin density plots and a qualitative molecular orbital diagram with canonical a_2 and b_1 ligand orbitals for reference (Figure 5a). First, **Cu-1** is best described as an antiferromagnetically coupled Cu^{II} corrole radical cation. The strong coupling (1236 cm^{-1}) between the Cu^{II} and the ligand radical accounts for the diamagnetic nature of the compound. The presence of a Cu^{II} centre is demonstrated by XPS, and is corroborated by the spin density plot (Figure 5b) that shows one α electron (black) in $d_{x^2-y^2}$ and one β electron (gray) in the corrole b_1 orbital.

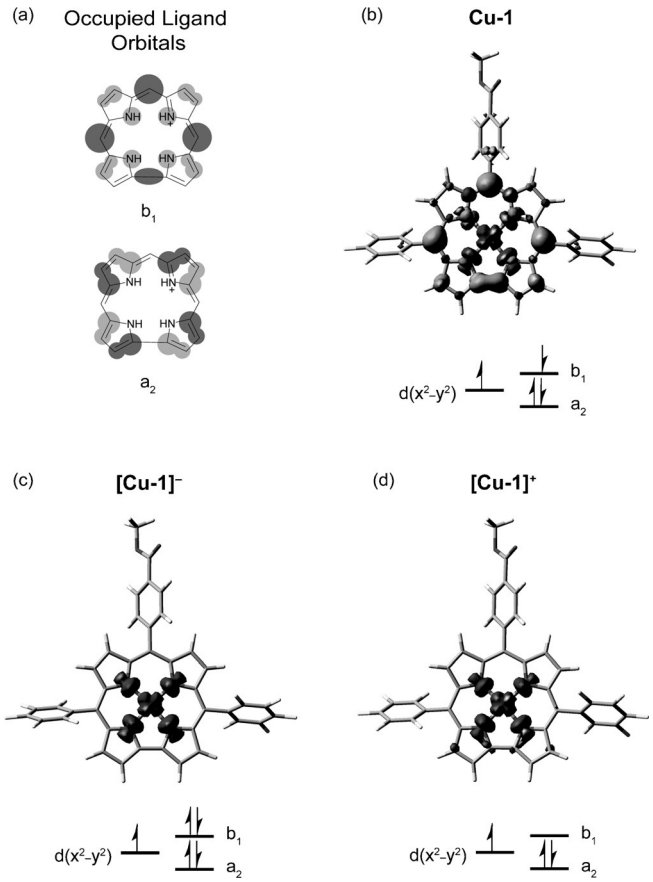

Figure 5. a) Canonical occupied corrole ligand orbitals: HOMO (b_1) and HOMO−1 (a_2), adapted from Ref. [20]. To illustrate the electronic structure of each derivative examined in this study, the calculated spin density plot and orbital occupancy is provided: b) singlet **Cu-1**, c) doublet $[\mathbf{Cu\text{-}1}]^-$, and d) doublet $[\mathbf{Cu\text{-}1}]^+$.

Both $[\mathbf{Cu\text{-}1}]^-$ and $[\mathbf{Cu\text{-}1}]^+$ have a single unpaired electron in $d_{x^2-y^2}$, as demonstrated by EPR, XPS, and corroborated by the spin density plots in Figure 5c and d. Thus, $[\mathbf{Cu\text{-}1}]^-$ is best described as a Cu^{II} $corrole^{3-}$ (closed shell, trianionic ligand), while $[\mathbf{Cu\text{-}1}]^+$ is a Cu^{II} $corrole^-$. The latter is a more satisfying electronic structure description than the recently proposed Cu^{IV} corrole complex;[13] our data for $[\mathbf{Cu\text{-}1}]^+$ is nearly identical to that reported for the proposed Cu^{IV} corrole. Our electronic structure formulations are consistent with those proposed by Ghosh on the basis of computational studies.[29] As a result, the reversible one electron reduction and oxidation are both ligand-based. It has been previously demonstrated that both of these processes are dependent on the identity of the *meso* substituents. The half-wave potential of the reduction shifts 160 mV, while that of the oxidation shifts 240 mV upon varying the substituent at the 4-position of the *meso* aryl ring from methoxy to trifluoromethyl.[14] In that study, Ghosh concluded that the electron was removed from a corrole orbital with substantial density at the *meso* positions (i.e., the b_1 orbital). For comparison, the metal-centred Mn^{III}/Mn^{II} reduction wave shifts only 50 mV by changing the 4-position of the *meso* aryl rings on the porphyrin ligand from methoxy to fluoro.[30]

We have presented a series of complementary spectroscopic experiments in order to assign the electronic structure of Cu corroles. We find that the ground state of Cu corroles is best described as an antiferromagnetically coupled Cu^{II} corrole radical cation, consistent with computational predictions. Strikingly, we demonstrate that the Cu^{II} oxidation state is maintained upon oxidation and reduction of the complex, with the macrocycle bearing the oxidizing and reducing equivalents. The Cu^{II} centre is preserved in each of these derivatives, underscoring the non-innocence of the corrole ligand in these complexes.

Acknowledgements

This work is supported by the U.S. Department of Energy Office of Science, Office of Basic Energy Sciences under Award No. DE-SC0009758. Funds were also provided by the TomKat Foundation. C.M.L. acknowledges the National Science Foundation's Graduate Research Fellowship Program and D.C.P. acknowledges a Ruth L. Kirchenstein National Research Service award (F32GM103211). We thank Dr. Kwabena Bediako for helpful discussions of the electrochemical data and Dr. Ryan Hadt for assistance with DFT calculations. We thank Dr. Yu-Sheng Chen for assistance with X-ray crystallography at ChemMatCARS, APS. ChemMatCARS Sector 15 is principally supported by the NSF/DOE under grant number NSF/CHE-1346572 and under Contract No. DE-AC02-06CH11357.

Keywords: computational chemistry · copper corroles · electronic structure · ligand non-innocence · redox chemistry

How to cite: *Angew. Chem. Int. Ed.* **2016**, *55*, 2176–2180
Angew. Chem. **2016**, *128*, 2216–2220

[1] A. W. Johnson, I. T. Kay, *J. Chem. Soc.* **1965**, 1620–1629.
[2] A. W. Johnson, *Pure Appl. Chem.* **1971**, *28*, 195–217.
[3] N. S. Hush, J. M. Dyke, *J. Inorg. Nucl. Chem.* **1973**, *35*, 4341–4347.
[4] N. S. Hush, J. M. Dyke, *J. Chem. Soc. Dalton Trans.* **1974**, 395–399.

[5] S. Will, J. Lex, E. Vogel, H. Schmickler, J. P. Gisselbrecht, C. Haubtmann, M. Bernard, M. Gross, *Angew. Chem. Int. Ed. Engl.* **1997**, *36*, 357 – 361; *Angew. Chem.* **1997**, *109*, 367 – 371.
[6] M. Bröring, F. Brégier, E. C. Tejero, C. Hell, M. C. Holthausen, *Angew. Chem. Int. Ed.* **2007**, *46*, 445 – 448; *Angew. Chem.* **2007**, *119*, 449 – 452.
[7] A. B. Alemayehu, E. Gonzalez, L. K. Hansen, A. Ghosh, *Inorg. Chem.* **2009**, *48*, 7794 – 7799.
[8] K. E. Thomas, J. Conradie, L. K. Hansen, A. Ghosh, *Eur. J. Inorg. Chem.* **2011**, 1865 – 1870.
[9] K. E. Thomas, A. B. Alemayehu, J. Conradie, C. M. Beavers, A. Ghosh, *Acc. Chem. Res.* **2012**, *45*, 1203 – 1214.
[10] A. B. Alemayehu, L. K. Hansen, A. Ghosh, *Inorg. Chem.* **2010**, *49*, 7608 – 7610.
[11] K. Pierloot, H. Zhao, S. Vancoillie, *Inorg. Chem.* **2010**, *49*, 10316 – 10329.
[12] A. Alemayehu, J. Conradie, A. Ghosh, *Eur. J. Inorg. Chem.* **2011**, 1857 – 1864.
[13] W. Sinha, M. G. Sommer, N. Deibel, F. Ehret, M. Bauer, B. Sarkar, S. Kar, *Angew. Chem. Int. Ed.* **2015**, *54*, 13769 – 13774; *Angew. Chem.* **2015**, *127*, 13973 – 13978.
[14] I. H. Wasbotten, T. Wondimagegn, A. Ghosh, *J. Am. Chem. Soc.* **2002**, *124*, 8104 – 8116.
[15] I. Luobeznova, L. Simkhovich, I. Goldberg, Z. Gross, *Eur. J. Inorg. Chem.* **2004**, 1724 – 1732.
[16] C. Brückner, R. P. Briñas, J. A. K. Bauer, *Inorg. Chem.* **2003**, *42*, 4495 – 4497.
[17] S. Nardis, G. Pomarico, F. R. Fronczek, M. G. H. Vicente, R. Paolesse, *Tetrahedron Lett.* **2007**, *48*, 8643 – 8646.
[18] G. Pomarico, X. Xiao, S. Nardis, R. Paolesse, F. R. Fronczek, K. M. Smith, Y. Fang, Z. Ou, K. M. Kadish, *Inorg. Chem.* **2010**, *49*, 5766 – 5774.
[19] C. M. Lemon, D. G. Nocera, *Faraday Discuss.* **2015**, *185*, 249 – 266.
[20] C. M. Lemon, R. L. Halbach, M. Huynh, D. G. Nocera, *Inorg. Chem.* **2015**, *54*, 2713 – 2725.
[21] B. Le Guennic, T. Floyd, R. B. Galan, J. Autschbach, J. B. Keister, *Inorg. Chem.* **2009**, *48*, 5504 – 5511.
[22] F. A. Cotton, J. L. Eglin, C. A. James, R. L. Luck, *Inorg. Chem.* **1992**, *31*, 5308 – 5315.
[23] F. A. Cotton, J. L. Eglin, B. Hong, C. A. James, *Inorg. Chem.* **1993**, *32*, 2104 – 2106.
[24] W. E. Keyes, W. E. Swartz, T. M. Loehr, *Inorg. Chem.* **1978**, *17*, 3316.
[25] P. C. Healy, S. Myhra, A. M. Stewart, *Jpn. J. Appl. Phys.* **1987**, *26*, L1884 – L1887.
[26] A. M. Romine, N. Nebra, A. I. Konovalov, E. Martin, J. Benet-Buchholz, V. V. Grushin, *Angew. Chem. Int. Ed.* **2015**, *54*, 2745 – 2749; *Angew. Chem.* **2015**, *127*, 2783 – 2787.
[27] J. P. Snyder, *Angew. Chem. Int. Ed. Engl.* **1995**, *34*, 80 – 81; *Angew. Chem.* **1995**, *107*, 112 – 113.
[28] A. C. Tsipis, *RSC Adv.* **2014**, *4*, 32504 – 32529.
[29] K. E. Thomas, H. Vazquez-Lima, Y. Fang, Y. Song, K. J. Gagnon, C. M. Beavers, K. M. Kadish, A. Ghosh, *Chem. Eur. J.* **2015**, *21*, 16839 – 16847.
[30] K. M. Kadish, M. M. Morrison, *Bioelectrochem. Bioenerg.* **1976**, *3*, 480 – 490.

Received: September 30, 2015
Revised: November 10, 2015
Published online: January 6, 2016

